Spontaneous coherent microwave emission and the sawtooth instability in a compact storage ring

U. Arp, G. T. Fraser, A. R. Hight Walker, and T. B. Lucatorto

Physics Laboratory, National Institute of Standards and Technology, Gaithersburg, Maryland 20899

K. K. Lehmann

Department of Chemistry, Princeton University, Princeton, New Jersey 08544

K. Harkay, N. Sereno, and K.-J. Kim

Advanced Photon Source, Argonne National Laboratory, Argonne, Illinois 60439

Strong evidence for self-excited emission of coherent synchrotron radiation in the microwave spectral region was observed at the Synchrotron Ultraviolet Radiation Facility (SURF III) electron storage ring at the NIST. The microwave emission between 25 and 35 mm was dominated by intense bursts of radiation. The intensity enhancement during these bursts was on the order of 10 000 to 50 000 over the incoherent value. The shape, width, and period of the bursts depend strongly on the operational parameters of the storage ring. Coherent microwave emission was observed only when the beam was unstable, namely, during bunch-length relaxation oscillations. We report on the measurements of the microwave bursts, and correlate the data with signals from a beam monitor electrode and photodiode detector. The coherent enhancement of the radiation intensity is ascribed to spontaneous self-induced microbunching of the electrons within the bunch.

I. INTRODUCTION

Self-excited coherent microwave synchrotron radiation was first observed in an electron storage ring at the Synchrotron Ultraviolet Radiation Facility SURF II [1,2]. Microwave radiation between 25 and 35 mm was emitted in intense bursts, with a periodicity dependent on machine conditions. Later, Carr *et al.* [3] reported the detection of spontaneous coherent synchrotron radiation in the mm wavelength range at the National Synchrotron Light Source VUV ring at Brookhaven National Laboratory. The period of the microwave bursts at SURF coincided strikingly with the period of bunch length relaxation oscillations, the latter first reported by Rakowsky [4,5], strongly suggesting a connection between the two effects. In this paper, we report on detailed measurements of the microwave intensity carried out while simultaneously collecting signals from a capacitive beam monitor electrode (BME) and from a photodiode system after SURF was upgraded to version III [6]. Simulations of the relaxation oscillations, or sawtooth instability, compare well with the BME data and reveal the time development of internal bunch structure, suggesting a mechanism for the coherent microwave emissions.

Following the formalism of Nodvick and Saxon [7], the intensity of synchrotron radiation at wavelength λ emitted by a bunch of N_e electrons is

$$P = P_0(N_e + N_e^2 f), \qquad (1)$$

where P_0 is the power emitted by a single electron [8] and f is a form factor, given by

$$f = \left(\int \cos(2\pi z/\lambda) S(z) \, dz \right)^2. \qquad (2)$$

In Eq. (2), $S(z)dz$ is the probability of finding electrons between z and $z + dz$. If we denote l_b as the bunch length, i.e., the interval over which $S(z)$ is non-negligible, then f takes on values from zero for wavelengths $\lambda \ll l_b$ (incoherent) to unity for $\lambda \gg l_b$ (coherent). Equations (1) and (2) show that a density modulation on the scale of λ can lead to an enhancement of the synchrotron radiation. Since a typical storage ring operates with N_e on the order of 10^{10}, even a very small amplitude Fourier component in the structure of the electron bunch can produce large enhancements in the radiation output through the N_e^2 dependence. The second term in Eq. (1) is usually referred to as the coherent synchrotron radiation (CSR).

In linear accelerators, the existence of CSR has been demonstrated utilizing the short electron bunches in linear accelerators passing through a single bend magnet [9–14] and has also been used to deduce the bunch length [15] and shape [16] for diagnostics purposes. Theoretical accounts include Nodvick and Saxon [7], Schiff [17], Michel [18], Klepikov and Ternov [19], Saldin *et al.* [20], and Wiedemann [21].

CSR in compact electron storage rings with short bunches has been predicted [22] but has not been directly observed. Observation of CSR is hampered by the shielding effect due to the small height of the vacuum chamber [23,24]. The suppression is effective for $\lambda \gtrsim \lambda_{th}$, where

$$\lambda_{th} = 2\sqrt{\frac{3h^3}{\pi\rho}} \,. \tag{3}$$

Here ρ is the bend radius and h is the chamber full height. The condition that the CSR be observable, $l_b \le \lambda_{th}$, becomes

$$\frac{12h^3}{\pi\rho l_b^2} \ge 1 \,. \tag{4}$$

This condition is normally not satisfied for high-energy storage rings.

At SURF, by Eq. (3), coherent emission at wavelengths greater than 67 mm would be completely suppressed by the 100 mm vertical height of the vacuum chamber. Furthermore, the 38 mm diameter of the vacuum extraction ports will transmit up to only about 50 mm wavelength, which is the TM_{01} cutoff. The full width at half maximum bunch length at SURF III was measured to be 400 mm at 331 MeV. Therefore, coherent emissions at wavelengths of the order of the bunch length are suppressed. However, given the observed microwave emission between 25 and 35 mm, CSR is not ruled out if there is some form of microbunching, e.g., if there is a density modulation in this case of the order of $1/10$ the bunch length. In this case, the inequality (4) can be satisfied by replacing l_b by l_m, the length of the microbunch. Such high-frequency structure may develop through beam-excited wakefields produced by the interaction between the beam and coupling impedances in the ring.

Relaxation oscillations of the bunch length have long been observed in the SURF ring, first reported by Rakowsky [4,5]. The period of these oscillations is observed to coincide with the period of the microwave bursts [1,2] both in broad and fine temporal detail, strongly suggesting a correlation. Relaxation oscillations are often referred to as sawtooth instabilities due to the shape of the time evolution of the bunch length. Early works by Sacherer [25] and others first described the thresholds for such bunch lengthening, then called microwave instabilities. A number of recent papers (e.g., Heifets [26], Wille [27], and Mosnier [28]) more rigorously describe the dynamics of sawtooth instabilities.

The increase in energy spread during the bunch length oscillations also causes the horizontal beam size to change through dispersion. The sawtooth instability can therefore generate intensity fluctuations in the synchrotron radiation, depending on the optics used in a given application. This motivates the present effort to understand and suppress the instability at SURF.

In this paper, we first describe the typical operation parameters for SURF. Then, the various diagnostic devices are discussed in some detail. This is followed by the results of experiments in which a number of signals were measured simultaneously. These demonstrate the close correlation of the sawtooth instability with the microwave bursts. Finally, we discuss a model that reproduces most of the features of the experimental results and offers an explanation of the origin of the microwave bursts.

II. SURF STORAGE RING

At SURF, the entire vacuum chamber is inside a single dipole magnet that keeps the electrons on a circular orbit based on the weak focusing principle [21]. Electrons can be stored at energies from 10 to about 380 MeV.

The magnetic lattice of the weak focusing accelerator is completely determined by the orbital radius $\rho_0 = 0.8382$ m and the magnetic field index $n = \frac{\rho_0}{B_0}\frac{\partial B}{\partial r}|_{r=\rho_0}$, where B is the magnetic guide field and the subscript refers to the values for the ideal orbit. The orbital frequency for SURF III is $f_0 = 56.923$ MHz, and the frequency of the driving rf field is $f_{rf} = 113.846$ MHz, leading to two bunches of electrons circulating in the vacuum chamber. Typical injection currents for SURF III are presently 350 to 450 mA. At a beam energy of 330.7 MeV and rf accelerating voltage, $V_{rf} = 13$ kV, the bunch length was determined with a fast photodiode (35 ps rise time) and a 1 GHz bandwidth oscilloscope to be 0.578 ns. This is equivalent to a FWHM of 400 mm. The FWHM horizontal and vertical beam sizes were found to be 2.1 mm by 0.026 mm, respectively, at 284.4 MeV [29]. This transverse beam size was determined by imaging the synchrotron radiation emitted by the electron beam onto a charged-coupled device camera, using a narrow band interference filter and taking into account diffraction and depth-of-field effects. Intrabunch or Touschek scattering [21] determines the electron beam lifetime at SURF III. The Touschek lifetime is proportional to the electron bunch volume. At SURF, the vertical betatron oscillation is excited and the vertical beam size increased to about 1 mm [4] to improve the lifetime. Typically, lifetimes of 1 to 3 h are achieved.

The last, very important parameter for the present experiments is the phase angle ϕ_{rf} between the rf generator and the rf accelerating cavity. Adjusting the phase alters the matching condition between the rf source and the cavity; this results in detuning the cavity for unmatched phase angles. The sawtooth instability and coherent microwave emission occur only at certain phase angles. Bench measurements of the rf cavity with a network analyzer show that the fundamental frequency shifts by ± 20 kHz and the higher-order mode (HOM) near $3f_{rf}$ shifts by ± 80 kHz while scanning ϕ_{rf}. Rakowsky [4,5] first suggested that the sawtooth instability at SURF could be attributed to a Robinson instability [30,31]. More recent measurements show that the rf cavity shunt impedance near $3f_{rf}$ is sufficient to give the instability growth rates observed [32]. In addition to tuning the cavity to the Robinson-unstable condition, it is notable that the amplitude of this HOM varies by almost a factor of 2. A list of SURF operating conditions is found in Table I, and a list of conditions for maximum instability amplitude is given in Table II.

TABLE I. Accelerator parameters for the SURF III machine conditions studied. The values in the table are calculated based on the energy and accelerating voltage. The measured rms bunch length is typically 40% greater than the natural value, and the measured synchrotron frequency is about 5% higher than the theoretical values listed.

Electron energy E (MeV)	Accelerating voltage V_{rf} (kV)	Radiative energy loss/turn U_i (keV)	Radiation damping time t_z (ms)	Relative energy spread σ_E/E	Bunch length σ_t (ns)	Synchronous phase angle ϕ_s (°)	Synchrotron frequency f_{syn} (kHz)
183.1	8.8	0.12	35.5	0.000 19	0.22	0.8	349
183.1	11.0	0.12	35.5	0.000 19	0.20	0.6	391
255.9	10.8	0.45	13.0	0.000 27	0.33	2.4	327
284.4	7.8	0.69	9.5	0.000 30	0.45	5.1	263
284.4	10.8	0.69	9.5	0.000 30	0.38	3.6	310
308.1	13.8	0.95	7.4	0.000 33	0.38	3.9	337
330.6	13.8	1.26	6.0	0.000 35	0.42	5.3	325

TABLE II. Period of the sawtooth instability and growth rate of the dominant coherent bunch phase oscillation modes ($m = 1, 2$) as a function of electron energy, beam current, cavity tune (relative to revolution harmonic: = on resonance, + above harmonic, − below harmonic), and rf transmission line phase angle. In data sets 1–3, only the current is varied (phase angle adjusted for maximum growth). In data sets 4–6, the cavity tune is varied. In data sets 7–11, the growth rates of the dominant modes are given for different machine conditions.

No.	Electron energy E (MeV)	Beam current I_B (mA)	Accelerating voltage V_{rf} (kV)	Cavity tune	Phase angle ϕ_{rf} (°)	Period Δt (ms)	Growth rate $m = 1$ (ms^{-1})	Growth rate $m = 2$ (ms^{-1})
1	284.4	10	7.8	=	46.9	>45	1.1	⋯
2	284.4	20	7.8	=	49.8	45	1.9	⋯
3	284.4	34	7.8	=	54.8	40	5.5	⋯
4	255.9	105	10.8	=	34.5	12.5	⋯	7.8
5	255.9	108	10.8	+	34.3	12	⋯	6.6
6	255.9	99	10.8	−	34.3	18	⋯	9.3
7	255.9	105	10.8	=	34.5	12.5	⋯	7.8
8	284.4	91.3	10.8	=	33.6	13.2	⋯	9.2
9	308.1	87.5	13.8	=	33.6	14	⋯	6.8
10	183.1	94	8.8	=	68.2	4.5	1.5	⋯
11	330.6	82.3	13.8	=	33.6	7.7	3.3	⋯

III. DIAGNOSTIC DEVICES

Here we describe the various diagnostic devices used in the experiments. The diagnostics used to measure the microwave emissions are described first. This is followed by the BME, from which the bunch length and beam spectra were obtained. Finally, the photodiode system is described, which measures horizontal beam size variations.

A. Microwave detection

The microwave emission from SURF III was measured using a broad band detector which integrates the total intensity from 7 to approximately 12 GHz. This emission was also spectrally resolved by using a low-gain microwave heterodyne receiver. The microwave radiation is collected using an X-band pyramidal horn located directly in front of a radiation port of the storage ring. The port of beam line 5 consists of a 38 mm diameter stainless steel tube oriented to collect the tangential forward synchrotron emission from the electron beam. The glass exit window is essentially transparent in the microwave region, and is located approximately 0.53 m from the tangent point of the electron beam. The microwave radiation is propagated down a 0.5 m long, Cu, X-band waveguide. The waveguide is designed for propagation of the TE$_{10}$ mode between 8.2 and 12.4 GHz and has a 6.56 GHz long wavelength cutoff. After propagating through the waveguide, the radiation travels through a 20 dB variable attenuator and ferrite isolator, and is then coupled out into a section of flexible coaxial cable using a waveguide-to-SMA (subminiature connector type A) adapter. For the spectral analysis, the microwave radiation is mixed with the output from a microwave frequency sweep synthesizer using an image-rejection mixer so that only one of the two possible difference frequencies results. The radio-frequency output of the mixer is passed through a 30 MHz narrow-band filter (2.1 MHz FWHM power bandwidth) and rectified into a dc voltage signal by a zero-bias 0.1 to 18 GHz, Schottky-diode detector. Detector-output-voltage versus synthesizer-frequency recordings are made using a digital oscilloscope with signal averaging capabilities. Intensity measurements were made by directly coupling the Schottky detector to an

amplifier to the waveguide-to-SMA adapter and recording the detector voltage as a function of time.

B. Bunch length and beam spectra

The SURF beam properties were monitored using the capacitive BME, also known as the Q probe. The BME is a 50 mm long section of rectangular S-band waveguide [32], with vertical and horizontal apertures of 41.3 and 76.2 mm, respectively. The BME signal was sampled on a digital oscilloscope together with the microwave power; the envelope of the BME signal on the oscilloscope is inversely proportional to the bunch length [32]. In addition, the BME signal was analyzed by a vector signal analyzer (VSA) to study the time evolution of the growth of synchrotron sidebands around the rf harmonics and by a spectrum analyzer to study the harmonic content of the bunch distribution.

C. Photodiode measurements

The bunch length oscillations during the microwave instability are accompanied by oscillations in the beam energy spread. The rms equilibrium bunch length is given by [21]

$$\sigma_s = \frac{\beta c |\eta_c|}{2\pi f_{\text{syn}}} \frac{\sigma_E}{E_0}, \tag{5}$$

with electron speed βc, momentum compaction $|\eta_c|$, synchrotron oscillation frequency f_{syn}, and the steady state energy spread $\frac{\sigma_E}{E_0}$. Since in our case we do not have simple constant Gaussian-bunch distribution, we choose to use a root mean square definition of the bunch length for the nonsteady state case:

$$\langle \sigma_s(t) \rangle_{\text{rms}} \approx \frac{\beta c |\eta_c|}{2\pi f_{\text{syn}}(t)} \frac{\sigma_E(t)}{E_0}. \tag{6}$$

The horizontal beam size is given by [21]

$$\sigma_x(t) = \sqrt{\epsilon_x \overline{\beta}_x + \left(\frac{\sigma_E(t)}{E_0}\right)^2 \overline{\eta}^2}, \tag{7}$$

where ϵ_x is the horizontal emittance, $\overline{\beta}_x$ is the average horizontal betatron function, and $\overline{\eta}$ is the average horizontal dispersion function. From Eqs. (6) and (7) it is clear that a change in bunch length will cause a change in horizontal beam size through the variation of the beam energy spread. This effect can cause intensity fluctuation in the collected synchrotron radiation at all wavelengths on the same time scale as the sawtooth instability.

In order to detect the effect of the relaxation oscillations on the horizontal beam size, we used the following setup: A lens imaged the radiation emitted by the electron beam onto an iris with variable opening. We placed a Hoya U-340 color glass filter in front of the iris and a silicon photodiode detector behind it to collect the transmitted radiation. The filter glass transmission window FWHM was

85 nm centered at 340 nm with a maximum transmittance of 75%. The photodiode signal was fed into a current amplifier and observed on the same digital oscilloscope as the BME and microwave power. If the iris is overfilled the transmitted intensity will vary with the beam size, leading to a signal proportional to the bunch length or beam energy spread.

IV. EXPERIMENTAL RESULTS

We performed several experiments where the various diagnostic signals were measured simultaneously to observe correlations and gain insight as to the origin of the coherent radiation enhancement and possible self-induced microbunching. A list of the varying machine conditions studied is found in Table I.

A. Coherent microwave bursts and the sawtooth instability

Figure 1 displays an example of the three simultaneously sampled signals: the integrated microwave power (top), BME (middle), and the photodiode system
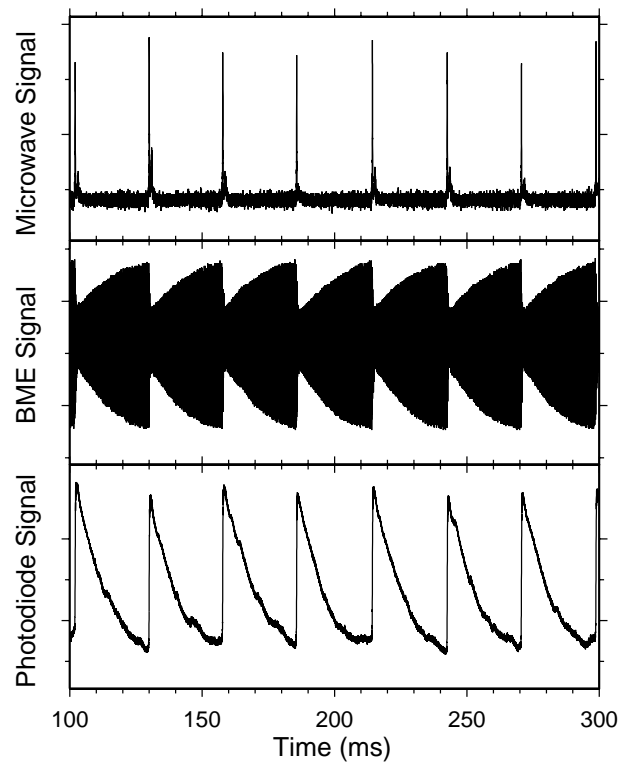

FIG. 1. Top: microwave signal; middle: beam monitor electrode signal; bottom: photodiode signal. The data were collected at $E_0 = 255.9$ MeV, $I_B = 87.6$ mA, $V_{\text{rf}} = 10.7$ kV, and $\phi_{\text{rf}} = 32.4°$. The time correlation between the different signals is very clearly exhibited. The period of the microwave power bursts is 27.9 ms. The FWHM of the main microwave bursts is about 0.13 ms. A second much smaller peak follows with 1 ms delay and FWHM 0.34 ms. The signal levels are omitted because they are not meaningful, since they depend strongly on the collection electronics.

(bottom). All three signals were collected simultaneously on the same digital oscilloscope, and the phase coincidence between the three signals is obvious. First, since the envelope of the BME signal is inversely proportional to the bunch length [32] the microwave bursts appear just after the bunch is longitudinally contracted and starts to blow up. The simulations of Migliorati *et al.* [33] predicted this behavior. Second, comparing the BME and photodiode signals reveals that the photodiode signal is proportional to the bunch length, which grows by up to a factor of 2 before the beam is stabilized. The machine condition for this measurement is described in the caption. The period of the bursts is 27.9 ms over the whole collected time span. The main microwave emission peak has a width of 0.13 ms FWHM, followed by a smaller peak with a delay of 1 ms and FWHM 0.34 ms.
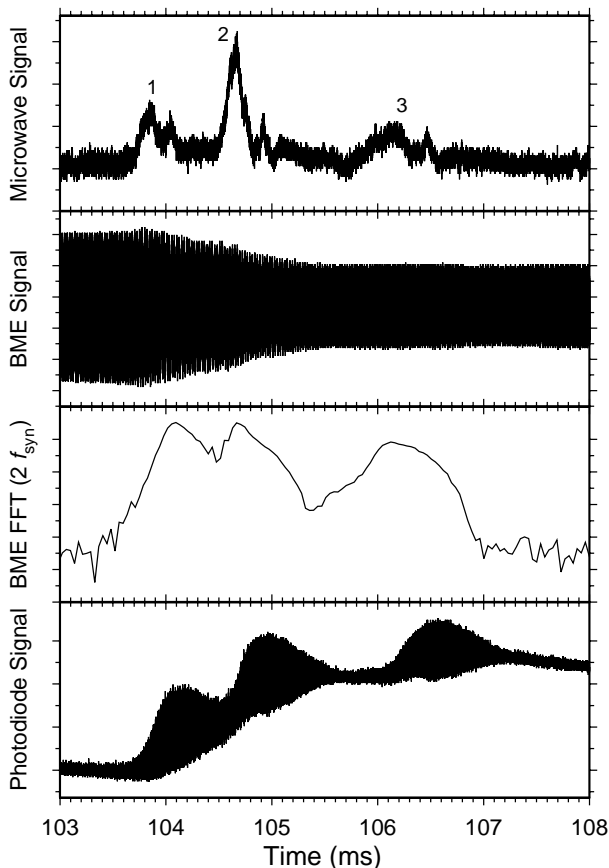
Figure 2 shows similar data on a much shorter time scale and slightly different rf phase (condition No. 4 in Table II, 90–100 mA). Here a main peak with FWHM 0.12 ms dominates the microwave emission, but several smaller structures precede and follow, which are correlated with shapes in the photodiode signal. A most striking correlation is seen with features in the BME spectrum, also shown in Fig. 2. The spectrum shows the amplitude vs time of the $2f_\text{syn}$ synchrotron sideband, which is the signature of the quadrupole bunch phase oscillation mode. The microwave bursts are almost exactly correlated in both time and duration with the rise of the quadrupole synchrotron harmonic power. Interestingly, the third burst occurs after the bunch length has blown up, an indication that internal bunch dynamics continue to be driven by the instability. High-frequency structure in the form of multiple higher-order synchrotron sidebands is shown in Fig. 3, which is a fast-Fourier transform of the BME signal, shown near the peak of the first blowup in Fig. 2. This structure gives indirect evidence that the bunch distribution filaments into microbunches during the bunch blowup. Direct confirmation of microbunching would require measurement in the time domain, such as with a streak camera.

A third example is shown Fig. 4. Here the microwave bursts are chaotic in nature. The data in this figure were collected at $E_0 = 183.1$ MeV (condition No. 10 in Table II). In this case, both the dipole and quadrupole synchrotron oscillation harmonics in the BME signal (not shown) are very closely correlated with the bursts. We performed experiments at several electron energy, beam current, and phase angle combinations to explore cross correlations (see Table II for details).
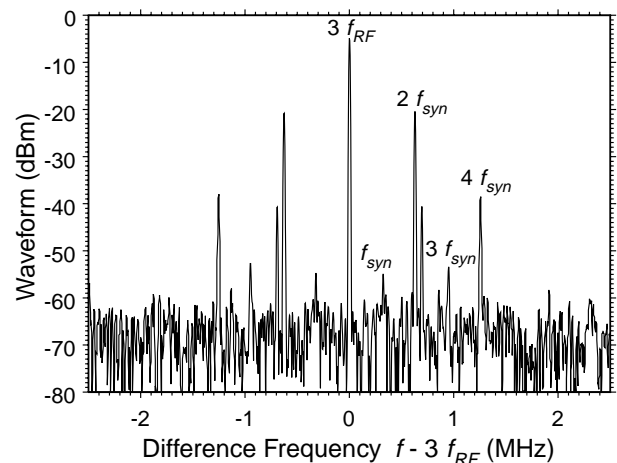

FIG. 2.   Top: microwave signal; second: BME signal; third: Fourier transform of BME signal, centered on $2f_\text{syn}$; bottom: photodiode signal. The data were collected at $E_0 = 255.9$ MeV, $I_B = 90$ mA, $V_\text{rf} = 10.8$ kV, and $\phi_\text{rf} = 34.5°$. The top signal shows that there is a main microwave burst (peak 2: FWHM 0.12 ms) and two dominant smaller peaks (peak 1: delay $\Delta t = -0.8$ ms, FWHM 0.15 ms; peak 3: $\Delta t = 1.5$ ms, FWHM 0.36 ms). These bursts are clearly correlated with the amplitude of the quadrupole synchrotron sideband in the BME spectrum (see also Fig. 3) and features in the photodiode signal. The signal levels are omitted because they are not meaningful, since they depend strongly on the collection electronics.

FIG. 3.   Rich harmonic content of beam, showing multiple synchrotron sidebands around $3f_\text{rf}$. This spectrum is measured near the peak of the first blowup of the quadrupole mode in Fig. 2. The dominant quadrupole mode appears to be split; the signal associated with the first blowup has shifted in frequency after growing in amplitude, while the signal associated with the second blowup begins to rise.
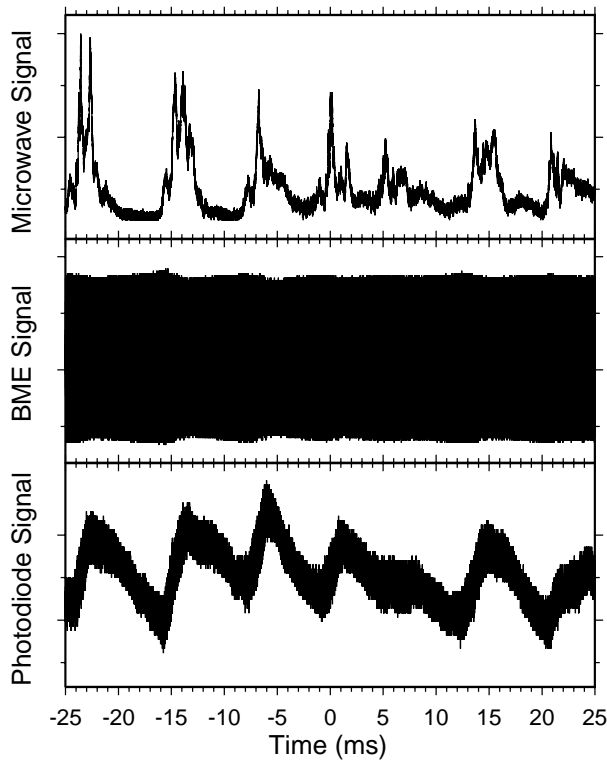
FIG. 4. Top: microwave signal; middle: beam monitor electrode signal; bottom: photodiode signal. The data were collected at $E_0 = 183.1$ MeV, $I_B = 105.5$ mA, $V_{rf} = 10.9$ kV, and $\phi_{rf} = 67.0°$. At this lower energy the microwave bursts are not as regular in time and shape. Their behavior is rather chaotic. Surprising here is that the bursts do not seem to be connected with strong changes in bunch length; however, they are correlated with dipole and quadrupole modes in the BME spectrum (not shown). The signal levels are omitted because they are not meaningful, since they depend strongly on the collection electronics.

B. Microwave spectra

The microwave emission is spectrally resolved using the heterodyne receiver described earlier. All microwave spectra were recorded at $E_0 = 255.9$ MeV with beam currents between $I_B = 98.7$ and 121.0 mA. Figure 5 shows the results for five measurements with different center frequencies and a span of about 300 MHz. The first measurement around the center frequency of 8 GHz was performed without a preamplifier. All following measurements were done using a preamplifier (the power scales are not adjusted). The plot in Fig. 5 has two *x* axes: the bottom one is the frequency of the emitted radiation and the top one is that frequency divided by the rf frequency of SURF, giving the number of the harmonic. Because SURF is operated with two equally filled bunches, the radiation is emitted at harmonics of twice the revolution frequency (harmonic number 2).
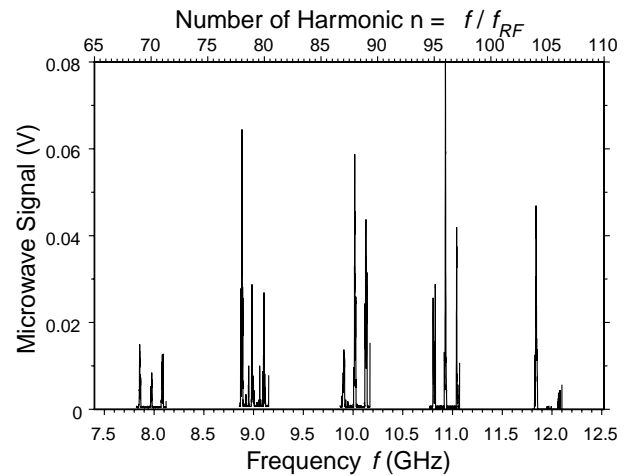

FIG. 5. Heterodyne spectra of the microwave emission from SURF III between 7.8 and 12 GHz. All spectra were recorded at $E_0 = 255.9$ MeV with beam currents between $I_B = 98.7$ and 121.0 mA. Not all harmonics were recorded. Each spectrum corresponds to the average of approximately 1000 sweeps of the local microwave oscillator. The oscillator is continuously swept over a 300 MHz interval at a rate of ∼10 Hz and the resulting spectra are added using a digital oscilloscope. The plot has two *x* axes: the lower is the frequency of the emitted radiation and the upper is the frequency divided by twice the orbital frequency giving the number of harmonic of the peaks. All spectra were recorded using a preamplifier except for the three peaks at the lowest frequency.

C. Microwave power enhancement

For the microwave enhancement measurements, a 30 dB amplifier was coupled directly to the attenuator, which then was fed into the Schottky diode detector. Then several measurements with different attenuation and scope settings were performed to account for nonlinearities in the detection system. From a comparison of measurements with 0 and 20 dB attenuation we could deduce the noncoherent synchrotron radiation intensity level to be 0.000 15 V. With 0 dB, the coherent intensity was 1.489 V, leading to an enhancement factor of approximately 10 000. A second measurement with 20 dB attenuation corresponded to a coherent signal level of about 7 V, leading to an enhancement of about 47 000. Without additional measurements it is very hard to estimate the uncertainties in these measurements because, e.g., the coupling efficiency of the detection system is not known and is difficult to determine. The power measurements utilized the integrated microwave intensity in the whole spectral window from 7 to approximately 12 GHz.

D. Spectrally analyzed BME signal

The BME signal was not only fed into a digital oscilloscope, but also into a spectrum analyzer to explore the harmonic content of the electron bunch. If microbunching is

abundant, the harmonic content in the BME spectrum will change during coherent emission. Therefore we triggered a spectrum analyzer (SA) with the microwave signal and indeed found significant enhancement above 2 GHz in the BME spectrum when the bursts occur (3 GHz maximum frequency range on SA). The envelope of the harmonics clearly shows that the beam develops a very non-Gaussian shape.

The BME signal was analyzed using the VSA to obtain details of the time evolution of the bunch length and growth of the coherent bunch phase oscillation modes that are determined by the internal degrees of freedom. The results are summarized in Table II. Depending on machine conditions, either the $m = 1$ dipole synchrotron mode or the $m = 2$ quadrupole mode is dominant (phase angle adjusted for maximum bunch lengthening). In the first set in Table II, the growth rate scales linearly with the bunch current, as expected, when everything else is fixed. The dipole mode is dominant and the sawtooth period is inversely proportional to the growth rate. In the second set in the table, the growth rate changes as expected when moving the tuner. When the tuner is pulled out, the cavity volume is increased, shifting the HOM frequencies down such that the impedance at the upper synchrotron sideband increases, and the instability growth rate increases. The coherent, unstable modes saturate at a higher amplitude, resulting in a larger bunch blowup. When the tuner is pushed in, the cavity volume decreases, shifting the HOM frequencies up and reducing the impedance, the beam is more stable and the growth rate decreases. Consequently, the coherent modes grow to a lower oscillation amplitude before saturating, causing a smaller bunch blowup. In this case, the quadrupole mode is dominant and now the sawtooth period is proportional to the growth rate.

E. Instability modeling

At SURF, high shunt impedance and quality factors measured for the HOMs make the rf cavity the most likely source of coupling impedance to induce the instability. In addition, detuning the cavity by adjusting the phase angle ϕ_{rf} also drives the sawtooth instability. The SURF cavity is a quarter-wave structure with HOMs only near the odd harmonics of the fundamental. Bench measurements, confirmed by MAFIA calculations, show that the HOMs are slightly above the odd harmonics [32]. This satisfies the condition for Robinson instability [30,31] at these higher harmonics, namely, that the impedance at the frequencies, $f = pf_{rf} \pm nf_0 \pm mf_{syn}$, is greater at the upper synchrotron sidebands (upper sign) than at the lower sidebands (lower sign). Here f_0 is the revolution frequency, f_{rf} is the rf frequency, f_{syn} is the synchrotron frequency, and $p = 0, 1, 2, \ldots$, $n = 0, 1$, and $m = 1, 2, \ldots$ are integers. Because the HOM impedances peak only near the even harmonics of f_0, only $n = 0$ modes can be excited, which means the bunches oscillate in phase. Since the

sawtooth instability was first reported at SURF, it has been observed in a number of other electron rings, most notably in the SLC damping rings [22,34] and the SPEAR electron storage ring at SLAC [35]. The modeling efforts to explain these observations can be compared to SURF.

To describe the SLC data [26,36], a broad band resonator impedance model is chosen with a frequency near the waveguide cutoff of the vacuum chamber. Because the wavelength of such a resonator impedance is short compared to the bunch length, it can directly give rise to high-frequency structure in the bunch and drive the microwave instability. However, relaxation oscillations can also occur for other impedance models. Limborg and Sebek [35] show experimentally and analytically that, in the case of SPEAR, a narrow band, rf cavity resonator tuned near the fundamental can also give rise to relaxation oscillations due to the Robinson instability. Robinson-like instabilities can occur at the HOMs as well, in particular, when these parasitic modes are near harmonics of the fundamental.

In an attempt to understand the experimental results at SURF, simulations were performed to address the main features of the longitudinal relaxation oscillations and explain the detailed dynamics of the phase space during the bunch blowup phase. We show that HOMs can indeed give rise to both high-frequency structure in the bunch and relaxation oscillations of the bunch length through the nonlinear evolution of the distribution. The vacuum chamber for SURF is large compared to the beam dimensions, thus the broad band impedance is not considered to be very important.

Particle tracking simulations of SURF were performed at various energies using the electron generation and tracking program ELEGANT [37]. ELEGANT tracks each particle using the six-dimensional phase space. The code also has the ability to simulate radiation damping and quantum excitation in a computationally fast way [38]. The simulation results are processed and compared directly with the results of measurements previously described.

In the simulation, the input resonator fundamental and HOM impedance parameters were obtained from the cavity bench measurements, reproduced in Table III. The beam current used in the simulation was 97 mA distributed in two bunches each containing 0.85 nC (48.5 mA). The simulation used 10 000 macroparticles in each bunch and tracking proceeded for up to 3×10^6 turns for various beam energies. This was enough time to simulate a few damping periods at each beam energy.

The results for 256 MeV beam energy and 10.8 kV rf voltage illustrate how the simulation reproduced many features of the observations. The phase space evolution of particle momentum vs time showed not only the overall bunch length relaxation oscillations, but also the multiple, smaller blowups of synchrotron oscillations. In the initial blowup, a large part of the core of the phase space starts to execute synchrotron oscillations, which grow to

TABLE III.   Bench measurements of the SURF rf cavity fundamental and HOM parameters [32].

Frequency f (MHz)	Quality factor Q_L	Shunt impedance R_L (kΩ)	FWHM Δf (MHz)
113.8	680	12	0.17
342.0	540	3.1	0.63
571.8	190	0.7	3.0
797.5	230	0.6	3.5
1027	143	0.3	7.2
1257	193	0.4	6.5
1462	⋯	⋯	

large amplitude. After the initial blowup has filamented in the nonlinear rf potential, the core left behind blows up in a similar fashion. The filaments of higher-density, small-scale structure persist for many synchrotron periods. Finally, the modulation in the distribution completely decoheres in phase space after both blowup stages. Radiation damping reduces the bunch length and the cycle repeats on time scales close to that observed. Inclusion of the HOMs appears to account for the details of the multiple bursts. In all cases, the two bunches show the same dynamics, as expected, since this is the in-phase mode $n = 0$.

The time evolution of the bunches is shown in Fig. 6. The dynamics of the two bunches is almost identical; for clarity, only one bunch is shown. The relaxation period of the rms bunch length is very similar to that in data set 4 in Table II. Dipole oscillations occurring during the blowup are also evident in the average centroid offset, also shown in the figure. It should be noted that, experimentally, the sawtooth period is often irregular for high current, exhibiting secondary blowups similar to that near 15 ms in the simulation [32].
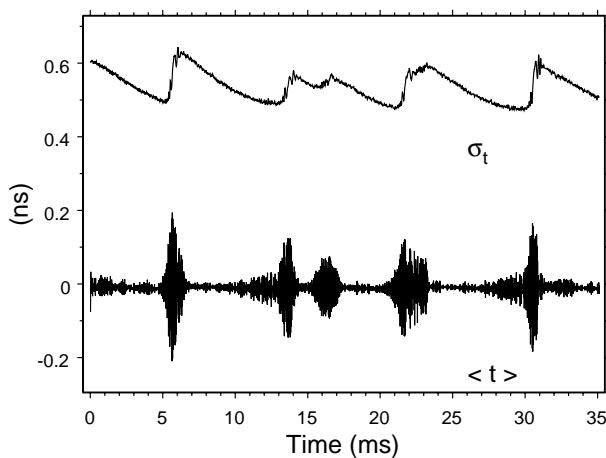

FIG. 6. Bunch time evolution in ELEGANT simulations of SURF. The top plot shows the relaxation oscillations of the rms bunch length, giving a period of 8 ms. The bottom plot shows the average centroid offset relative to the synchronous particle, showing dipole motion occurring during the blowup phase.
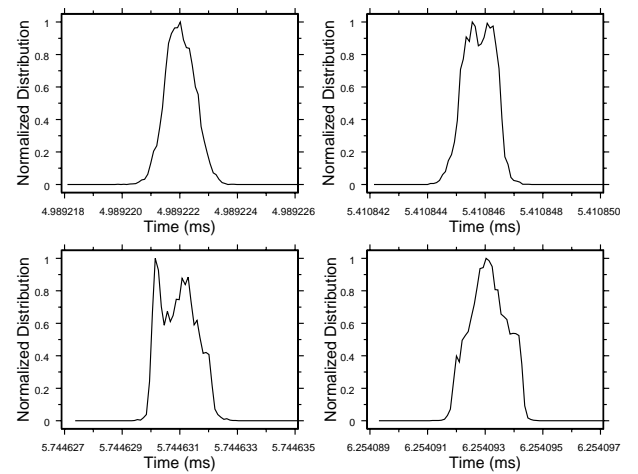

FIG. 7. Bunch distributions in ELEGANT simulations of SURF, just before, during, and after the blowup due to the instability, starting from the upper left. The time delay from the first to the second plot (upper right) is 0.4 ms, to the third (lower left) is 0.75 ms, and to the last (lower right) is 1.26 ms. The third plot especially shows high-frequency structure during the second mini blowup. The bunch elongation due to the blowup in the model was on the order of 50% whereas a factor of approximately 2 was actually observed.

The bunch longitudinal distribution was obtained by generating histograms of the phase space distribution in time. Figure 7 shows the distribution just before, during, and after the blowup. The bunch clearly exhibits dipole motion as well as high-frequency structure. Analysis of the frequency structure of the distribution during the blowup period was performed. The high-frequency spectral content of the bunch distributions was computed, and shows the development of 1 to 3 GHz structure during the blowups. This is not, however, as high as the 7 to 12 GHz microwave emissions that were measured.

The phase space tracking analysis based on the rf cavity resonator model is able to account fairly well for the instability blowup observed, and is capable of producing microstructure on the bunch during the blowup period where enhanced radiation is observed. In addition, and especially interesting, the temporal features of multiple excitations of coherent bunch mode oscillations almost exactly match the multiple bursts of enhanced microwave radiation. However, this model is not complete. It does not explain why the dipole or quadrupole mode dominates for a given set of parameters, noted in the results in Table II. In addition, the simulation did not produce any spectral enhancement over the microwave band from 7 to 12 GHz described in the measurements. Additional modeling is planned to help address these discrepancies, e.g., adding the CSR wakefield computation to ELEGANT.

V. CONCLUSIONS

The coherent enhancement of microwave intensity at SURF III appears to be attributed to wakefield-induced,

self-driven microbunching during turbulent bunch length oscillations. The microwave bursts have the same period as the bunch length oscillations, and details of the temporal features of the bursts match simulations of the instability. From simultaneous measurements of the microwave output, a beam monitor electrode and a photodiode signal, we show that the microwave emission occurs just after the maximum bunch compression, at the onset of coherent bunch mode oscillations and as they saturate when the bunch length blowup starts. Coherent enhancement factors of 10 000 to 50 000 and the spectrally analyzed beam monitor signal support association of the coherent emission with microbunching. Simulations of the instability driven by rf cavity higher-order modes show the development of high-frequency features in the nonlinear time evolution of bunch mode oscillations that also suggests the possibility of microbunching. Also it has to be pointed out that under normal operating conditions SURF III is a quiet and stable source of synchrotron radiation, and the measurements reported here were possible only by detuning the accelerator.

ACKNOWLEDGMENTS

[1] G. T. Fraser, A. R. Hight Walker, U. Arp, T. Lucatorto, and K. K. Lehmann, in *Synchrotron Radiation,* edited by E. Fontes, AIP Conf. Proc. No. 417 (AIP, New York, 1997).

[2] A. R. Hight-Walker, U. Arp, G. T. Fraser, T. B. Lucatorto, and J. Wen, in *Accelerator-Based Infrared Sources and Applications,* edited by G. P. Williams and P. Dumas, SPIE Proceedings No. 3153 (SPIE–International Society for Optical Engineering, Bellingham, WA, 1997).

[3] G. L. Carr, S. L. Kramer, J. B. Murphy, J. LaVeigne, R. P. S. M. Lobo, D. H. Reitze, and D. Tanner, in *Proceedings of the 1999 Particle Accelerator Conference, New York,* edited by A. Luccio and W. MacKay (IEEE, Piscataway, NJ, 1999), p. 134.

[4] G. Rakowsky and L. R. Hughey, IEEE Trans. Nucl. Sci. **26**, 3845 (1979).

[5] G. Rakowsky, IEEE Trans. Nucl. Sci. **32**, 2377 (1985).

[6] M. L. Furst, R. M. Graves, A. Hamilton, L. R. Hughey, R. P. Madden, R. E. Vest, W. S. Trzeciak, R. A. Bosch, L. Greenler, and P. R. D. Wahl, in *Proceedings of the 1999 Particle Accelerator Conference, New York* (Ref. [3]), p. 2388.

[7] J. S. Nodvick and D. S. Saxon, Phys. Rev. **96**, 180 (1954).

[8] J. Schwinger, Phys. Rev. **75**, 1912 (1949).

[9] T. Nakazato *et al.,* Phys. Rev. Lett. **63**, 1245 (1989).

[10] Y. Shibata *et al.,* Nucl. Instrum. Methods Phys. Res., Sect. A **301**, 161 (1991).

[11] Y. Shibata *et al.,* Phys. Rev. A **44**, R3445 (1991).

[12] K. Ishi *et al.,* Phys. Rev. A **43**, 5597 (1991).

[13] Y. Shibata, K. Ishi, T. Takahashi, F. Arai, M. Ikezawa, K. Takami, T. Matsuyama, K. Kobayashi, and Y. Fujita, Phys. Rev. A **44**, R3449 (1991).

[14] E. B. Blum, U. Happek, and A. J. Sievers, Nucl. Instrum. Methods Phys. Res., Sect. A **307**, 568 (1991).

[15] D. X. Wang, G. A. Kraft, E. Price, P. A. D. Wood, D. W. Porterfield, and T. W. Crowe, Appl. Phys. Lett. **70**, 529 (1997).

[16] G. Schneider, R. Lai, W. Walecki, and A. J. Sievers, Nucl. Instrum. Methods Phys. Res., Sect. A **396**, 283 (1997).

[17] L. I. Schiff, Rev. Sci. Instrum. **17**, 6 (1946).

[18] F. C. Michel, Phys. Rev. Lett. **48**, 580 (1982).

[19] N. P. Klepikov and I. M. Ternov, Nucl. Instrum. Methods Phys. Res., Sect. A **308**, 113 (1991).

[20] E. L. Saldin, E. A. Schneidmiller, and M. V. Yurkov, Nucl. Instrum. Methods Phys. Res., Sect. A **398**, 373 (1997).

[21] H. Wiedemann *Particle Accelerator Physics* (Springer-Verlag, New York, 1993).

[22] R. L. Warnock and K. Bane, SLAC Technical Report No. SLAC-PUB-95-6837, 1995.

[23] S. A. Kheifets and B. Zotter, CERN SL Report No. 95-43, 1995.

[24] R. L. Warnock, KEK Technical Report No. KEK 90-21, 1991.

[25] F. J. Sacherer, IEEE Trans. Nucl. Sci. **24**, 1393 (1977).

[26] S. A. Heifets, Phys. Rev. E **54**, 2889 (1996).

[27] K. Wille, Nucl. Instrum. Methods Phys. Res., Sect. A **393**, 18 (1997).

[28] A. Mosnier, Nucl. Instrum. Methods Phys. Res., Sect. A **438**, 225 (1999).

[29] U. Arp, Nucl. Instrum. Methods Phys. Res., Sect. A **462**, 568 (2001).

[30] K. Robinson, Cambridge Electron Accelerator Technical Report No. CEA-11, 1956.

[31] K. Robinson, Cambridge Electron Accelerator Technical Report No. CEAL-1010, 1964.

[32] K. C. Harkay and N. S. Sereno, Argonne National Laboratory Technical Report No. LS-268, 1998.

[33] M. Migliorati, L. Palumbo, G. Dattoli, and L. Mezi, Nucl. Instrum. Methods Phys. Res., Sect. A **437**, 134 (1999).

[34] B. V. Podobedov, SLAC Technical Report No. SLAC-R-543, 1999.

[35] C. Limborg and J. Sebek, Phys. Rev. E **60**, 4823 (1999).

[36] R. Baartman and M. D'Yachkov, in *Proceedings of the 1995 Particle Accelerator Conference, Dallas, Texas* (IEEE, Piscataway, NJ, 1996), p. 3119.

[37] M. Borland, http://www.aps.anl.gov/asd/oag/manuals/elegant_ver14.1/elegant.html.

[38] M. Borland (private communication).